Journal of the European Ceramic Society 43 (2023) 5195–5206

Contents lists available at ScienceDirect

Journal of the European Ceramic Society

journal homepage: www.elsevier.com/locate/jeurceramsoc

Processing of ZrB_2 tribo-ceramics by reactive spark plasma sintering of ZrH_2+2B subjected to high-energy pre-ball-milling

Jesús López-Arenal [a], Bibi Malmal Moshtaghioun [a,*], Diego Gómez-García [a], Angel L. Ortiz [b,*]

[a] Departamento de Física de la Materia Condensada, Universidad de Sevilla, 41080 Sevilla, Spain
[b] Departamento de Ingeniería Mecánica, Energética y de los Materiales, Universidad de Extremadura, 06006 Badajoz, Spain

ARTICLE INFO

Keywords:
ZrB_2
Reactive spark plasma sintering
High-energy ball-milling
Tribo-ceramics
Sliding wear

ABSTRACT

The reactive spark plasma sintering (RSPS) of monolithic ZrB_2 ceramics from ZrH_2+2B powder mixtures subjected to shaker pre-milling was investigated, and compared with other three sintering approaches. It was found that RSPS is optimal at 1850 °C, which results in fully-dense ZrB_2 ceramics with ~20 GPa hardness. Comparatively, at 1850 °C RSPS from the simply-mixed ZrH_2+2B powder mixture, SPS from the commercial ZrB_2 powder, and SPS from the shaker-milled ZrB_2 powder result in non-dense (76.7–86.7%) and softer (6.0–11.8 GPa) ZrB_2 ceramics. Furthermore, the optimally RSPS-ed ZrB_2 ceramic was subjected to unlubricated sliding-wear tests against diamond under 40 N load for 1000 m of sliding, demonstrating that it is a promising tribo-ceramic that only undergoes mild tribo-oxidative wear at 10^{-8} $mm^3/(N{\cdot}m)$ in the form of a slight plasticity-dominated two-body abrasion with eventual formation and partial loss of a self-lubricating and protective oxide tribolayer.

1. Introduction

ZrB_2 is a member of the ultra-high-temperature ceramic (UHTC) family [1–5], so called in virtue of their high melting points above 3000 °C, and doubtless the most investigated of them all. Indeed, over the last two decades a substantial knowledge base has been accumulated on the synthesis, sintering, thermal and mechanical properties, and oxidation of monolithic ZrB_2 ceramics and ZrB_2–based composites [6,7], especially with a view to their possible use in the field of extreme-environment engineering and, more particularly, in aerospace engineering (*e.g.*, hypersonic flight, atmospheric re-entry, and scramjet and rocket propulsion) [8]. However, they could also be used as substitutes for other structural ceramics in many other applications, particularly in the field of tribology. Although not as hard as other structural ceramics (*e.g.*, B_4C and SiC), these UHTCs are also very hard [9], which in principle makes them suitable for applications requiring wear resistance (*e.g.*, bearings, valves, and nozzles) [10]. Their ultra-refractoriness and high thermal conductivity are in fact a plus for resisting and alleviating, respectively, frictional heating. Also, their high electrical conductivity allows them to be used as substitutes for metals in tribological applications requiring electrical contact, and to be machined into complex shapes by electrical discharge machining rather than with diamond tools. Not surprisingly, there have already been studies on the wear behaviour of monolithic ZrB_2 ceramics and ZrB_2–based composites under varied tribological conditions (*e.g.*, loads, tribo-part, and medium) and contact geometries (*e.g.*, sliding and scratch) [11–24].

However, a limiting factor for the widespread use of these UHTCs in tribological applications is their poor densification capability because porosity is a major microstructural source of degradation of the wear resistance and other engineering properties of ceramics. Indeed, they are extremely difficult to sinter, more as monolithic than as composites, so they are more often fabricated by hot pressing (HP) and spark plasma sintering (SPS) than by pressureless sintering (PS). Importantly, reactive sintering (RS), in which a mixture of elemental powders reacts and densifies during the sintering cycle itself, has also been used as an alternative to the classical sintering (PS, HP, or SPS) of ZrB_2 powders in the case of monoliths, or of powder mixtures of ZrB_2 with other ceramics in the case of composites. Table 1 lists previous work on the RS of monolithic ZrB_2 ceramics [25–28]. Despite it being difficult to draw conclusions from the comparison of these few studies, it seems that RS of ZrB_2 benefits from the application of pressure and fast heating (*i.e.*, the utilisation of SPS), the use of ZrH_2 reactant instead of Zr reactant, and the shaker pre-milling treatment. Also importantly, RS has been shown

* Corresponding authors.
E-mail addresses: mali_moshtagh@us.es (B.M. Moshtaghioun), alortiz@unex.es (A.L. Ortiz).

https://doi.org/10.1016/j.jeurceramsoc.2023.04.047
Received 18 March 2023; Received in revised form 10 April 2023; Accepted 20 April 2023
Available online 23 April 2023

Table 1
Summary of conditions and results of previous studies on the RS of monolithic ZrB_2 ceramics.

Reference	Sintering technique	Powder mixture composition	Powder mixture preparation	Sintering conditions	Densification degree
[25]	pressureless reactive sintering	Zr+2B	shaker milling	1 h/2000 °C	72%
[25]	pressureless reactive sintering	Zr+2B	shaker milling	1 h/2200 °C	79%
[25]	pressureless reactive sintering	Zr+2B	simply mixed	1 h/2200 °C	70%
[26]	reactive hot pressing	ZrH_2+2B	simply mixed	2 h/1900 °C/50 MPa	98.9%
[26]	reactive hot pressing	ZrH_2+2B	simply mixed	1 h/2050 °C/50 MPa	99.6%
[26]	reactive hot pressing	ZrH_2+2B	simply mixed	15 min/2100 °C/50 MPa	99.2%
[27]	reactive spark plasma sintering	Zr+2.1B	shaker milling	20 min/1900 °C/20 MPa/500 °Cmin^{-1}	87%
[27]	reactive spark plasma sintering	Zr+2.1B	shaker milling	20 min/1900 °C/50 MPa/500 °Cmin^{-1}	95%
[27]	reactive spark plasma sintering	Zr+2.1B	shaker milling	20 min/2000 °C/20 MPa/200 °Cmin^{-1}	96%
[28]	reactive spark plasma sintering	ZrH_2+2B	wet milling	10 min/1800 °C/50 MPa/100 °Cmin^{-1}	97.2%

Table 2
Set of ceramics fabricated and their fabrication conditions.

Sintering technique	Powder mixture used	Sintering temperature[a]	Number
reactive spark plasma sintering	shaker-milled ZrH_2+2B	1500–1900 °C in 50 °C steps	9
reactive spark plasma sintering	simply-mixed ZrH_2+2B	1850 °C	1
spark plasma sintering	commercial ZrB_2	1850 °C	1
spark plasma sintering	shaker-milled commercial ZrB_2	1850 °C	1

[a] Other sintering conditions are 100 °C/min heating ramp, 5 min soaking at peak temperature, and 50 MPa pressure.

to be comparatively more effective in producing dense monolithic UHTCs than more typical sintering approaches [26,29].

Given the above context, the present study was undertaken with three novel objectives in mind. The first objective was to investigate the RSPS of ZrB_2 from a ZrH_2+2B powder mixture subjected to shaker pre-milling, which has not yet been explored despite the few earlier studies [25–28] suggesting that this would be the ideal combination of reactants, pre-treatment, and sintering technique. The second objective was to compare under a common experimental platform the RSPS of ZrB_2 from the shaker-milled ZrH_2+2B powder mixture with RSPS of ZrB_2 from the simply-mixed ZrH_2+2B powder mixture, SPS of a typical commercial ZrB_2 powder, and SPS of the commercial ZrB_2 powder subjected to shaker pre-milling. Not only has this comparison between the four not yet been done, but also the two existing partial comparisons either took data from different studies [26] or were not for ZrB_2 (but for HfB_2 and TaB_2) [29]. The third objective was to investigate the unlubricated sliding-wear behaviour of the optimally RSPS-ed ceramic against diamond (to thus simulate the scenario of wear against a much harder tribo-part), which involves fundamental tests not as yet performed but necessary to assess the potential usefulness of these ceramics in tribological applications.

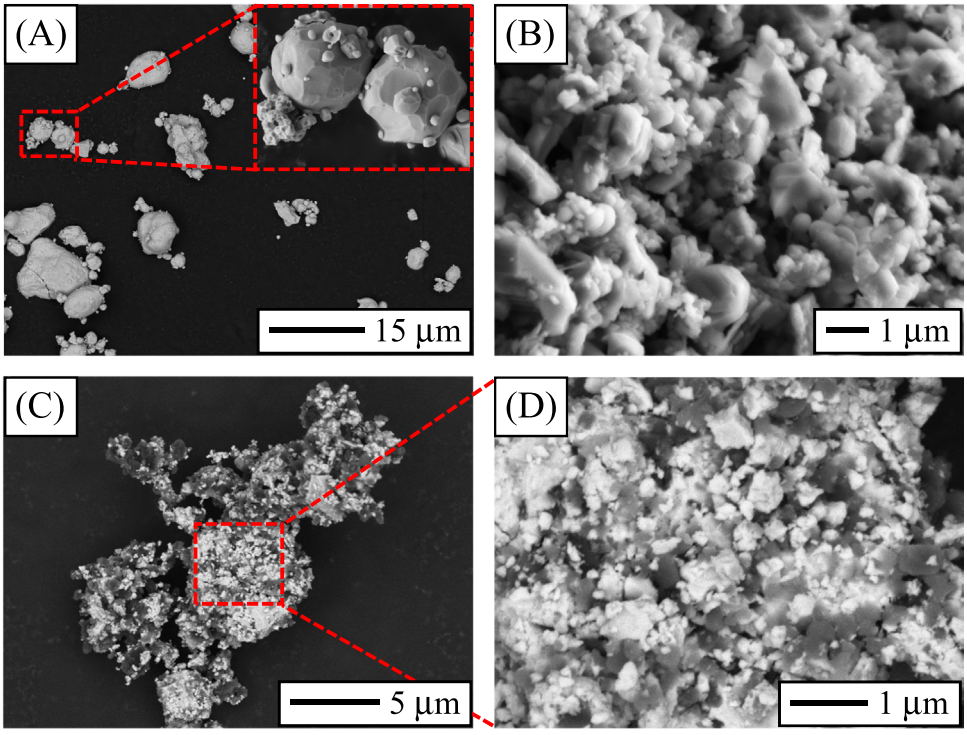

Fig. 1. FE-SEM images of the starting (A) ZrH_2 and (B) B powders as well as of (C-D) the ZrH_2+2B powder mixture subjected to shaker milling. Imaging of the powder mixture was done with backscattered electrons to differentiate between ZrH_2 (light particles) and B (dark particles).

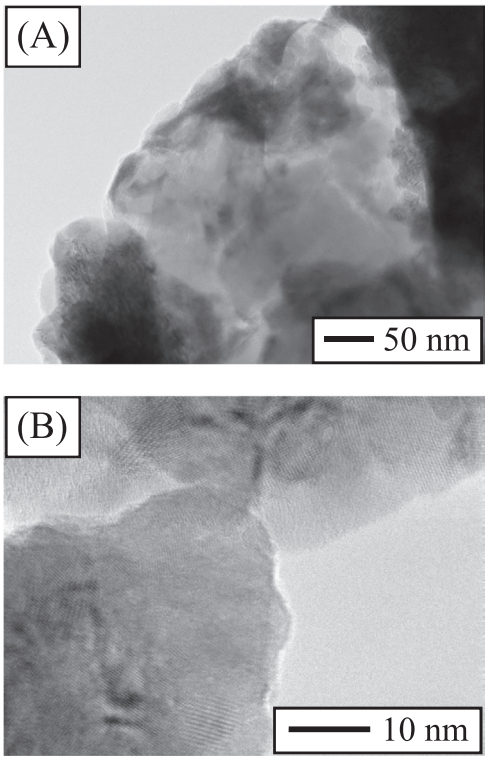

Fig. 2. TEM images of the ZrH_2+2B powder mixture subjected to shaker milling, taken within the agglomerates at (A-B) different locations and magnifications.

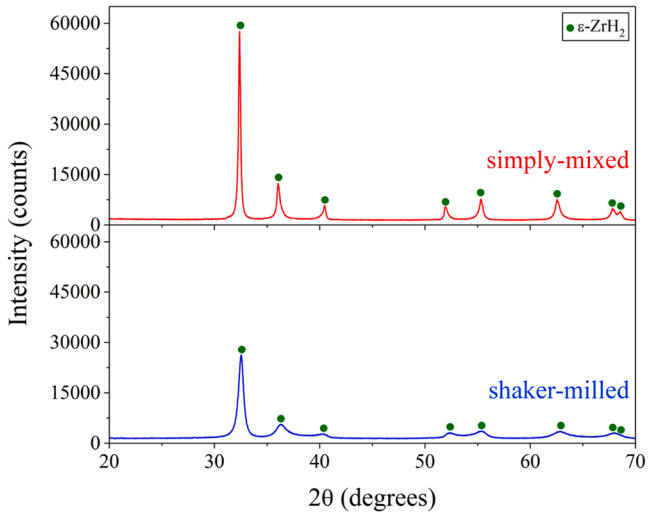

Fig. 3. XRD patterns of the simply-mixed and shaker-milled ZrH_2+2B powder mixtures. Peak assignations, as identified using the PDF2 database (PDF number 00–036–1339 for ε-ZrH_2), are included. The intensity scale is the same for the two XRD patterns to facilitate their direct visual comparison.

2. Experimental procedure

2.1. Processing and characterisations

Commercially available (MaTecK, Germany) powders of ZrH_2 (99.7% purity) and B (95% purity) were purchased, combined in molar ratio 1ZrH_2:2B, and subjected to dry high-energy ball-milling for 1 h in a shaker mill (Spex D8000, Spex CertiPrep, USA) at 1060 back-and-forth cycles/min using a hardened-steel container with WC balls (6.7 mm in diameter) under a ball-to-powder weight ratio of 4, in an inert atmosphere of ultrahigh-purity Ar to prevent oxidation of the powder mixture during milling. Also, a first sacrificial milling was performed, which has been shown to be effective in preventing the contamination of the powder mixture by the milling tools [30–35]. The shaker-milled ZrH_2+2B powder mixture was subsequently characterised using field-emission scanning electron microscopy (FE-SEM; FEI Teneo, FEI Inc., USA), transmission electron microscopy (TEM; Tecnai G^2 20 Twin, FEI Inc., The Netherlands), X-ray diffractometry (XRD; D8 Advance, Bruker AXS, Germany) under CuKα incident radiation, and thermogravimetry (TG; Labsys Evo, Setaram, France) coupled with differential thermal analysis (DTA; Labsys Evo, Setaram, France) under flowing Ar, and compared with the as-purchased ZrH_2 and B powders and with the simply-mixed ZrH_2+2B powder mixture.

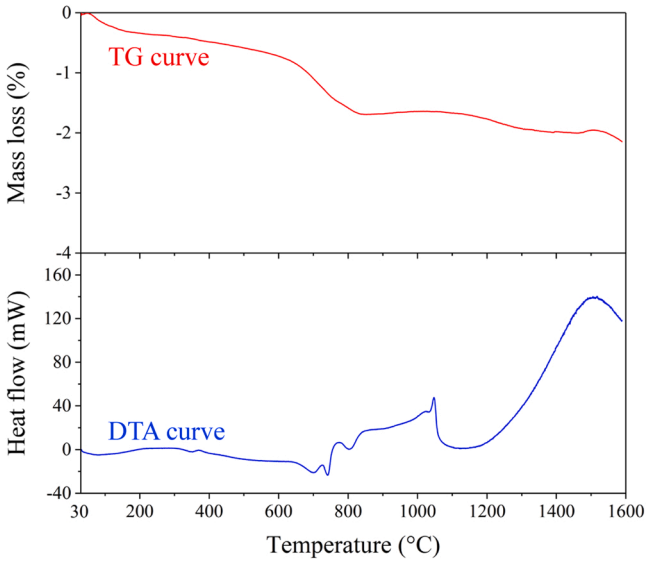

Fig. 4. Curves of TG and DTA (exothermic upwards) of the shaker-milled ZrH_2+2B powder mixture. The two curves were registered simultaneously as a function of the temperature in the range 25–1600 °C under heating at 10 °C/min in flowing Ar atmosphere.

The shaker-milled ZrH_2+2B powder mixture was then loaded into graphite dies (2.5 cm diameter) lined with graphite foils and covered by graphite blankets, and densified using an SPS furnace (HP-D-10, FCT Systeme GmbH, Germany) operated in dynamic vacuum at target temperatures in the range 1500–1900 °C (as measured by an axial pyrometer and reached at 100 °C/min), without intermediate holds, for 5 min under 75 MPa pressure (applied at 300 °C). The resulting ceramics were ground and diamond-polished to a 0.25-μm finish using conventional ceramographic procedures, and were characterised microstructurally by XRD, SEM (S-3600 N, Hitachi, Japan) on fracture surfaces and, selectively, FE-SEM on polished and electrochemically-etched surfaces (45 s at 0.4 mA/cm^2 in 0.05 M KOH solution), and water immersion porosimetry (*i.e.*, the Archimedes method). Also, their hardness was measured by Vickers indentation (Duramin, Struers A/S, Denmark). 10 indentations were performed for each material, at 9.8 N load, 40 μm/s load rate, and 20 s dwell time.

As reference for comparison, three additional powder batches were also prepared and RSPS-ed/SPS-ed. Two were a typical commercially available ZrB_2 powder (Grade B, H. C. Starck, Germany) used both in its as-received condition and shaker pre-milled under identical conditions as the ZrH_2+2B powder mixture. The third was the simply-mixed ZrH_2+2B powder mixture, which was homogenised in ethanol for 24 h and conveniently dried and deagglomerated. These three powder batches were RSPS-ed/SPS-ed under the optimal RSPS temperature of 1850 °C previously identified for the shaker-milled ZrH_2+2B powder mixture. Table 2 lists the 4 types of monolithic ZrB_2 ceramics fabricated

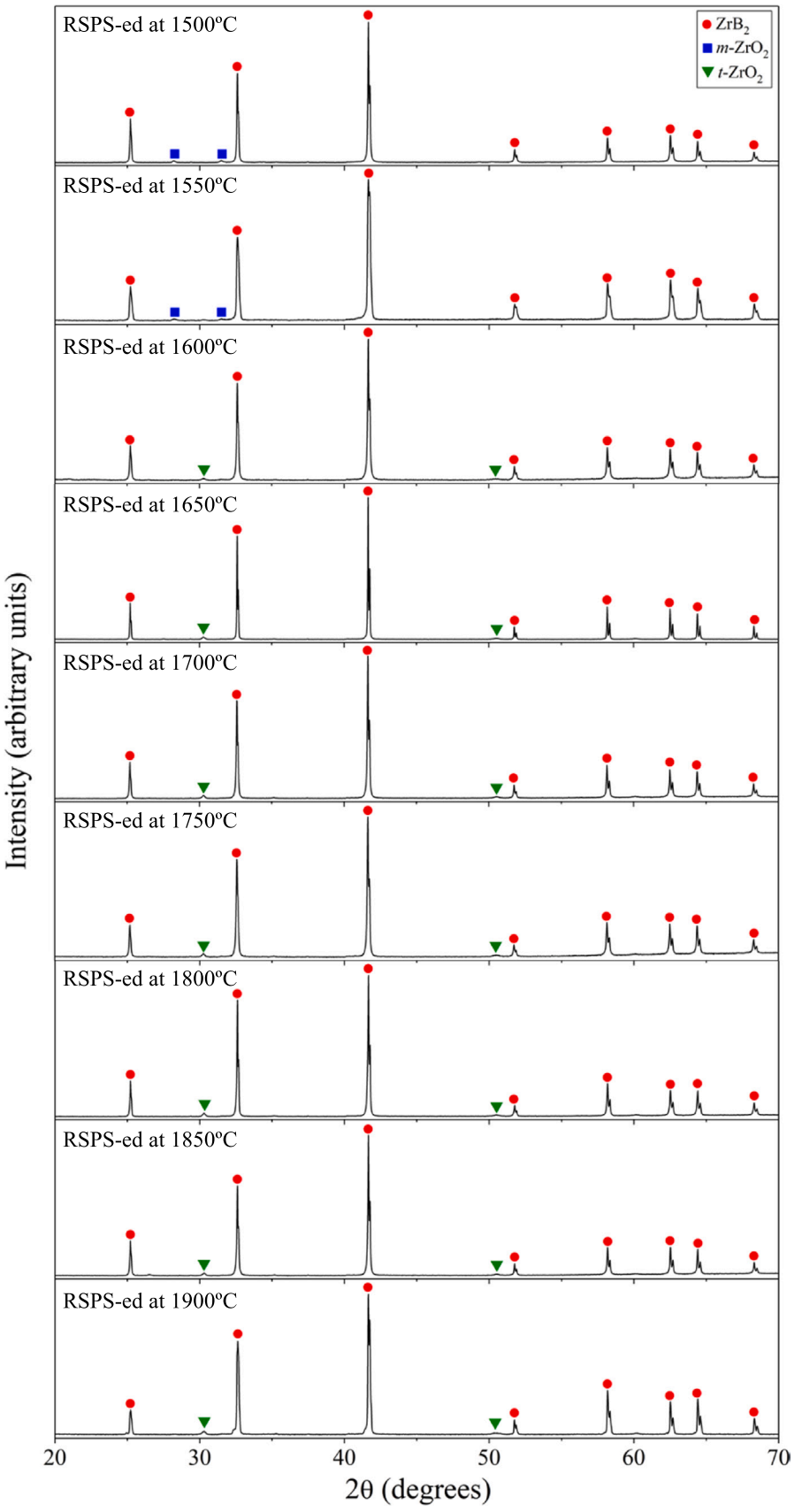

Fig. 5. XRD patterns of the nine ceramics fabricated by RSPS (for 5 min under 75 MPa) from the shaker-milled ZrH_2+2B powder mixture. The RSPS temperature is indicated. Peak assignations, as identified using the PDF2 database (PDF numbers 00–034–0423 for ZrB_2, 00–037–1484 for *m*-ZrO_2, and 00–050–1089 for *t*-ZrO_2), are included. The letters *m* and *t* mean monoclinic and tetragonal, respectively. The intensity scale is logarithmic to facilitate observation of the weaker peaks. Very weak ZrO_2 peaks have not been labelled.

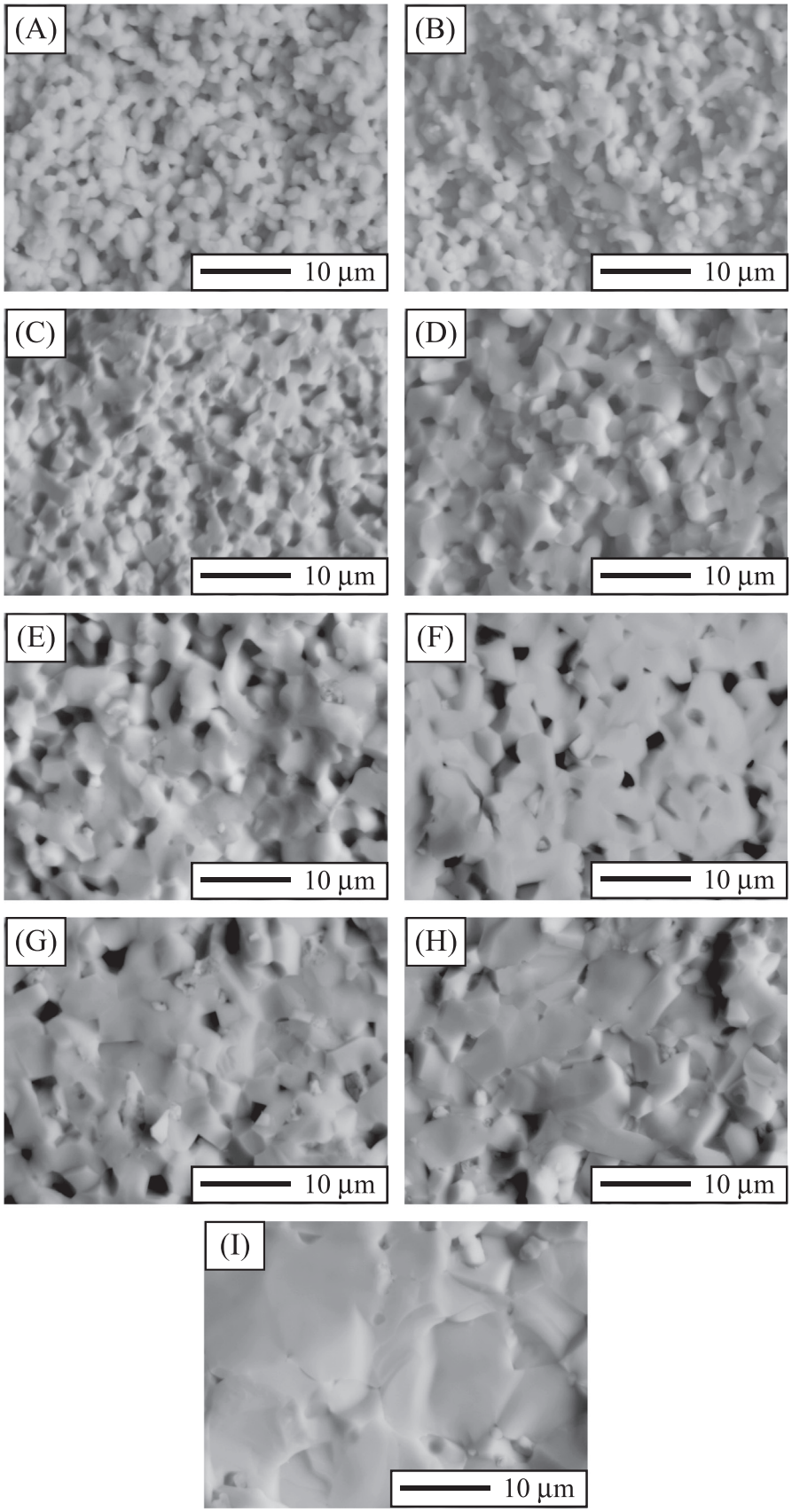

Fig. 6. SEM images of the fracture surface of the nine ZrB_2 ceramics fabricated by RSPS (for 5 min under 75 MPa) from the shaker-milled ZrH_2+2B powder mixture at (A) 1500 °C, (B) 1550 °C, (C) 1600 °C, (D) 1650 °C, (E) 1700 °C, (F) 1750 °C, (G) 1800 °C, (H) 1850 °C, and (I) 1900 °C. The magnification is the same to facilitate the direct visual comparison of microstructural features (porosities and grain sizes).

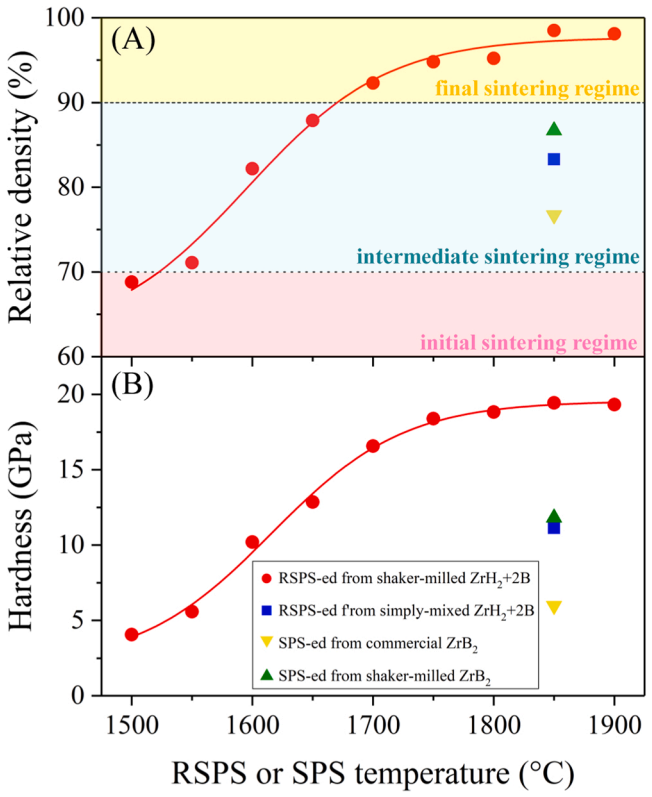

Fig. 7. Values of (A) relative density and (B) hardness as a function of their sintering temperature for the twelve ceramics fabricated. The dotted and dashed lines as well as the coloured boxes in (A) distinguish the regimes of initial, intermediate, and final sintering (*i.e.*, densification lower than 70%, between 70% and 90%, and more than 90%, respectively). Errors are smaller than the point size. The solid lines through the data are guides for the eye.

and their fabrication conditions.

2.2. Unlubricated sliding-wear tests and characterisations

The optimal of all ceramics fabricated was subjected to unlubricated sliding wear, under ambient conditions. Specifically, sliding-wear tests were done (MFT-3000, Rtec Instruments, USA), in duplicate, in the ball-on-disk configuration without external lubricant at 40 N load, 10 cm/s linear sliding speed, 2 mm track radius, and 1000 m total sliding distance, using 6.02 mm diameter diamond-coated SiC balls (Dball G10, Nova Diamant, UK) as counter-parts. The coefficient of friction (CoF) was continuously logged during the wear tests. The worn surfaces of the ZrB_2 ceramic were examined using different techniques. Specifically, digital optical microscopy (DOM; AM7915MZT-Edge, Dino-Lite, The Netherlands), optical microscopy (OM; Epiphot 300, Nikon, Japan), and optical profilometry (OP; Profilm 3D, Filmetric, USA) in white light interferometry mode were used to inspect the wear-induced macro-damage. OP was additionally used to compute the worn volume, and thence the specific wear rate (SWR) and the attendant wear resistance. Moreover, SEM together with energy-dispersive X-ray spectroscopy (EDS; flash Detector 3001, Röntec GmbH, Germany) were used to inspect the wear-induced micro-damage. The combination of DOM, OM, OP, and SEM/EDS allowed the wear mode and mechanism(s) to be identified.

3. Results and discussion

3.1. Characterisation of the shaker-milled powder mixture

Fig. 1 shows FE-SEM images of the as-received ZrH_2 and B powders

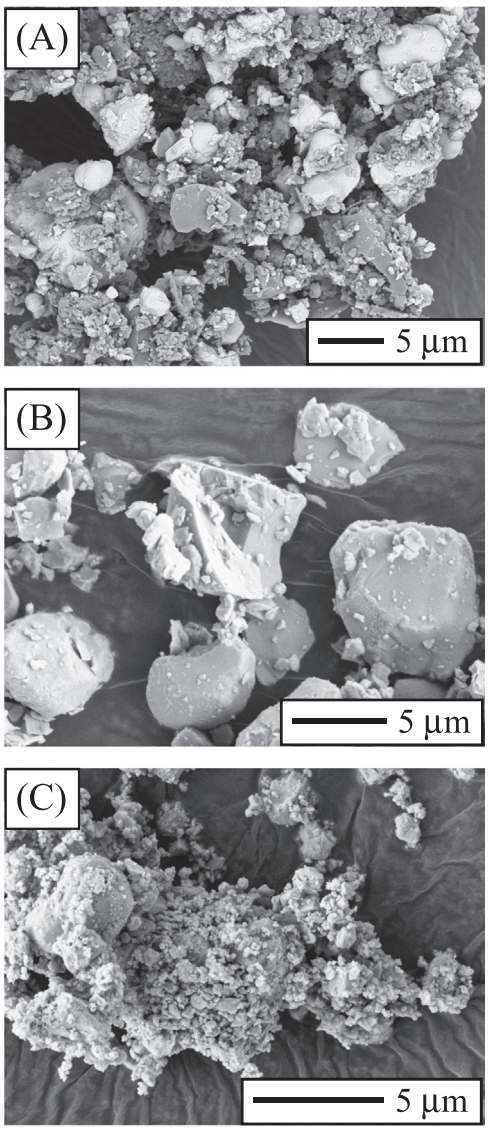

Fig. 8. FE-SEM images of the (A) ZrH_2+2B powder mixture prepared simply by wet homogenisation, (B) a typical commercial ZrB_2 powder, and (C) the commercial ZrB_2 powder subjected to the same shaker milling as the ZrH_2+2B powder mixture. Imaging of the powder mixture was done with backscattered electrons to differentiate between ZrH_2 (light particles) and B (dark particles).

as well as of the shaker-milled ZrH_2+2B powder mixture. It can be seen in Fig. 1A that the ZrH_2 powder comprises rounded particles with sizes ranging from less than one micron to more than ten microns, and in Fig. 1B that the B powder is finer and more uniform, with an apparent particle size in the submicrometric range. Comparatively, it can be seen in Fig. 1C-D that the shaker-milled ZrH_2+2B powder mixture is formed by micrometric agglomerates of ultrafine particles that are one and two orders of magnitude smaller than the B and ZrH_2 starting particles, respectively. The FE-SEM images of Fig. 1C-D, taken with backscattered electrons to have compositional contrast, also show a uniform dispersion of the two types of particles within the agglomerates (*i.e.*, ZrH_2 (lighter particles) and B (darker particles)), indicating that shaker milling, which is the most effective form of high-energy ball-milling [36], not only refined the particles' sizes, but also intimately mixed the ZrH_2 and B powders. Fig. 2 shows TEM images of the shaker-milled ZrH_2+2B powder mixture revealing that the agglomerates are compact but porous (Fig. 2A), and confirming that they contain ultrafine and even nanometric particles (Fig. 2B), indicative that they formed through short thermal excursion in the presence of pressure. This is because at the

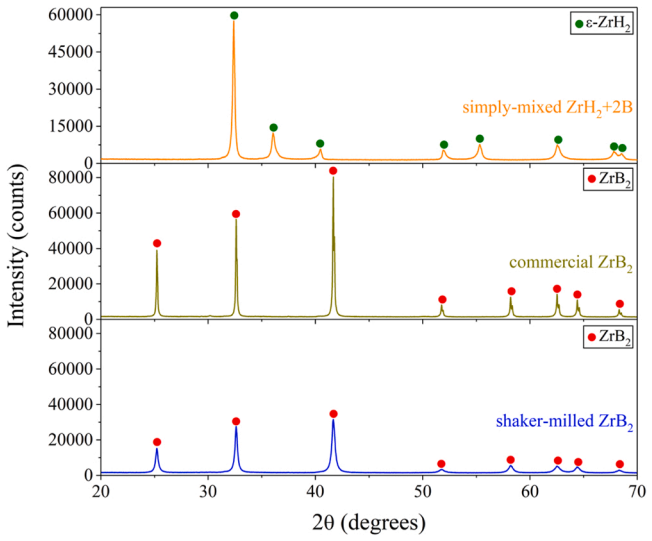

Fig. 9. XRD patterns of the simply-mixed ZrH_2+2B powder mixture, the commercial ZrB_2 powder, and the shaker-milled ZrB_2 powder, as indicated. Peak assignations, as identified using the PDF2 database (PDF numbers 00–036–1339 for ε-ZrH_2 and 00–034–0423 for ZrB_2), are included. The intensity scale is the same for the XRD patterns of the two ZrB_2 powders to facilitate their direct visual comparison. Very weak ZrO_2 peaks have not been labelled.

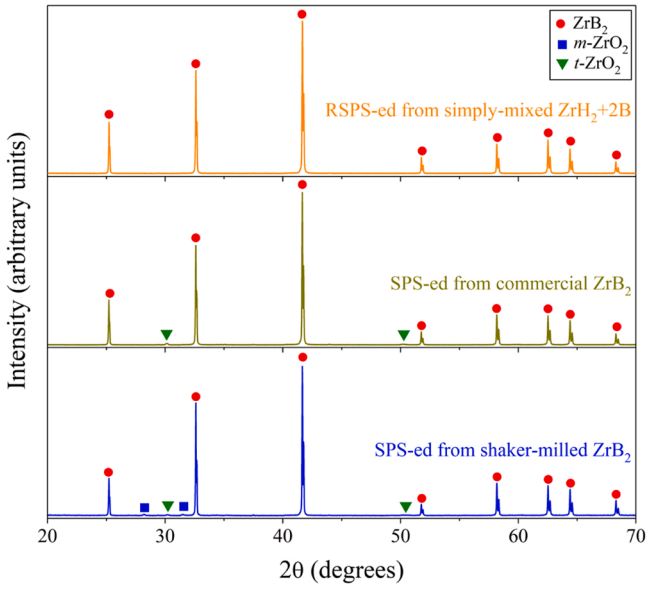

Fig. 10. XRD patterns of the three reference ceramics fabricated by RSPS at 1850 °C (for 5 min under 75 MPa) from the simply-mixed ZrH_2+2B powder mixture and by SPS at 1850 °C (for 5 min under 75 MPa) from both the commercial ZrB_2 powder and the shaker-milled ZrB_2 powder, as indicated. Peak assignations, as identified using the PDF2 database (PDF numbers 00–034–0423 for ZrB_2, 00–037–1484 for *m*-ZrO_2, and 00–050–1089 for *t*-ZrO_2), are included. Very weak ZrO_2 peaks have not been labelled.

collision site there is a local temperature spike of ~300 °C with the presence of high compressive stresses of ~6 GPa of very short duration of the order of 10^{-6}–10^{-5} s [37].

Fig. 3 shows the XRD patterns of both the simply-mixed and shaker-milled ZrH_2+2B powder mixtures. It is clear that the two have the same phase composition, with only crystalline ε-ZrH_2 plus amorphous B. Therefore, the absence of ZrB_2 in the shaker-milled ZrH_2+2B powder mixture rules out the occurrence of reaction between ZrH_2 and B during high-energy ball-milling. The two XRD patterns differ however in that the diffraction peaks are much broader and less intense after shaker milling, which is further evidence of particle size refinement and mechanical activation during high-energy ball-milling. Also importantly, the absence of WC peaks in the XRD pattern after shaker milling confirms the non-contamination of the ZrH_2+2B powder mixture by the milling tools, attributable to the first sacrificial milling depositing a layer of powder mixture on the WC balls and hardened-steel container [38].

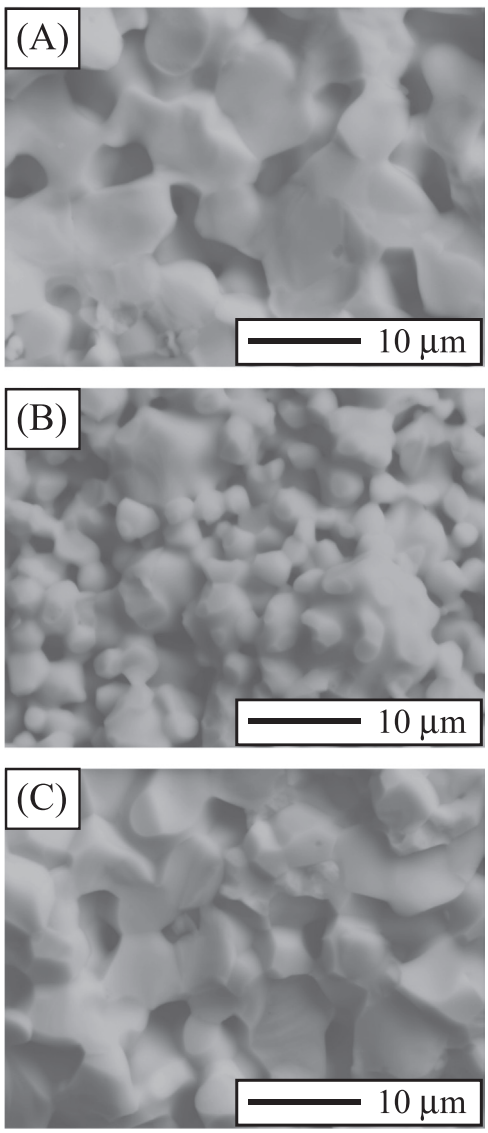

Fig. 11. SEM images of the fracture surface of the three reference ZrB_2 ceramics fabricated (A) by RSPS at 1850 °C (for 5 min under 75 MPa) from the simply-mixed ZrH_2+2B powder mixture and by SPS at 1850 °C (for 5 min under 75 MPa) from (B) the commercial ZrB_2 powder and from (C) the shaker-milled ZrB_2 powder. The magnification is the same and equal to that in Fig. 6 to facilitate the direct visual comparison of microstructural features (porosities and grain sizes).

Fig. 4 shows the TG–DTA curves of the shaker-milled ZrH_2+2B powder mixture registered at 10 °C/min in the temperature range 25–1600 °C in flowing Ar. It can be seen in the TG curve that the total mass loss is only ~2% wt%, and ~1.8% wt% when the initial loss of physisorbed water is excluded, and that this occurs during the first ~850 °C. This mass loss is simply due to the ZrH_2 decomposition because the reaction $ZrH_2 \rightarrow Zr + H_2(g)$ predicts the release of ~2.16 wt% of hydrogen gas that would imply a mass loss of ~1.75 wt% in the

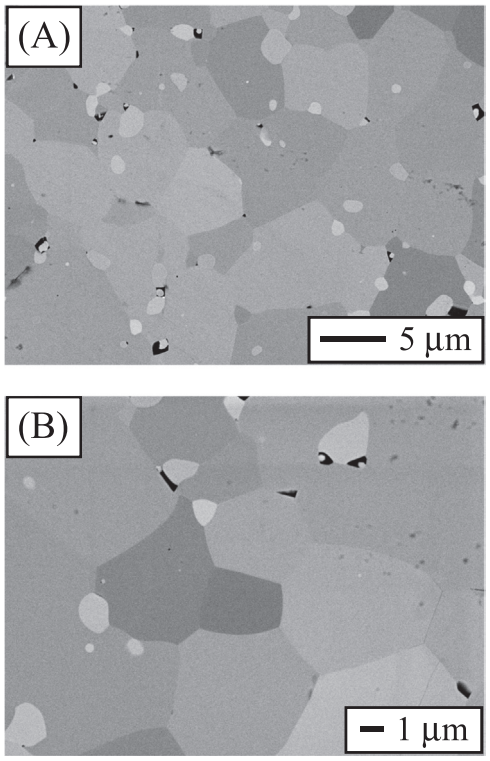

Fig. 12. FE-SEM images of the polished and electrochemically-etched surface of the ZrB_2 ceramic fabricated by RSPS at 1850 °C for 5 min under 75 MPa from the shaker-milled ZrH_2+2B powder mixture, taken at (A-B) different locations and magnifications. The larger, darker grains are ZrB_2, and the smaller, lighter grains are ZrO_2.

ZrH_2+2B powder mixture. The ZrH_2 decomposition is known to occur in various steps [39], which is also consistent with the shape of the TG curve. On the other hand, it can be seen in the DTA curve that two broad exothermic events occurred, the first in the temperature range ~750–1100 °C without a well-defined maximum, and the second from ~1200 °C onwards with a maximum at ~1500 °C. The former event comes accompanied by mass loss, and is thus due to the ZrH_2 decomposition ($ZrH_2 \rightarrow Zr+H_2(g)$). The latter event does not come accompanied by mass loss and releases much more heat, and is therefore attributable to the ZrB_2 formation reaction ($Zr+2B \rightarrow ZrB_2$). This, which is consistent with thermodynamic data [40], suggests that ZrB_2 should be the main phase in the RSPS-ed ceramics.

3.2. Optimisation of the RSPS temperature

Fig. 5 shows the XRD patterns of the 9 ceramics fabricated by RSPS from the shaker-milled ZrH_2+2B powder mixture at 1500–1900 °C for 5 min under 75 MPa pressure. It can be seen that they all contain essentially only ZrB_2, indicating that the expected reaction $ZrH_2+2B \rightarrow ZrB_2$ was completed at an RSPS temperature below 1500 °C. There are also traces (*i.e.*, <5 vol%) of ZrO_2, which is attributable to the slight spontaneous passivation of ultrafine ZrH_2 particles during placement of the dies in the chamber of the SPS furnace. In any case, what matters is that the reaction of ZrB_2 formation was completed at a lower temperature during RSPS than expected from the DTA curve in Fig. 4, which is not a surprise for two reasons. Firstly, at the heating rates used in both RSPS and DTA the reaction is governed by solid-state diffusion [27], and the reaction kinetics is therefore favoured by the faster heating and the pressure application as there is less particle growth and more intimate particle contact. Secondly, the actual temperature in the sample during RSPS is in fact higher than that measured by the axial optical pyrometer [41,42].

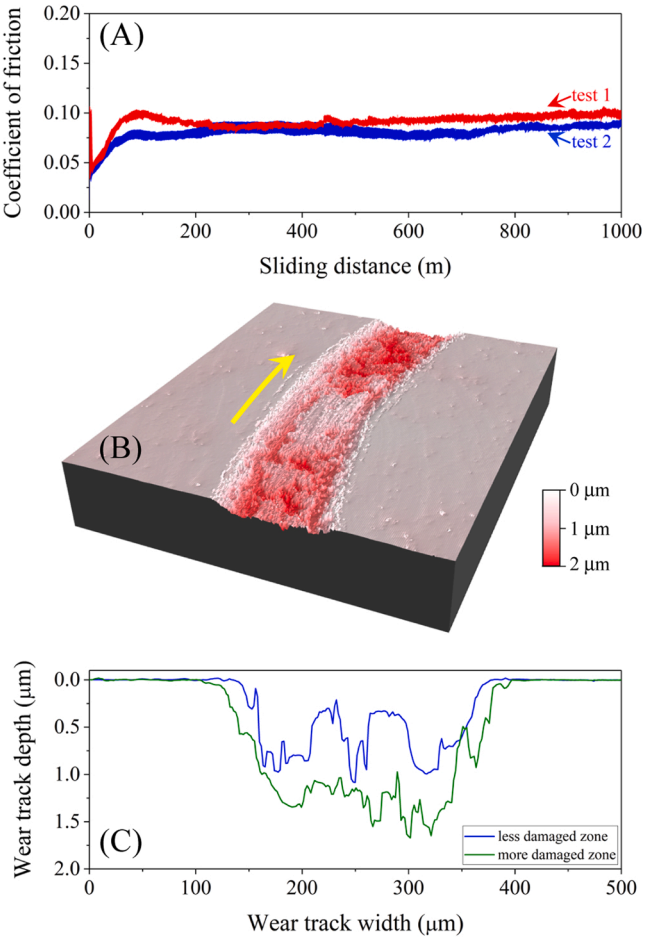

Fig. 13. Results deriving from the sliding-wear tests for the ZrB_2 ceramic fabricated by RSPS at 1850 °C (for 5 min under 75 MPa) from the shaker-milled ZrH_2+2B powder mixture. (A) Friction curves measured as a function of the distance slid, (B) 3-D image representative of the residual wear track at the conclusion of the wear tests, as obtained by OP, and (C) typical 2-D cross-sectional profiles extracted from zones with more and less damage of the wear tracks. The arrow in (B) denotes the sliding direction.

Fig. 6 shows SEM images of the fracture surface of the entire set of ZrB_2 ceramics fabricated by RSPS from the shaker-milled ZrH_2+2B powder mixture. The microstructural changes with increasing RSPS temperature are evident both in terms of degree of densification and of grain shape and size. Thus, it can be seen that the two ceramics RSPS-ed at 1500 °C and 1550 °C simply look like compacted rounded fine powder, that the two ceramics RPS-ed at 1600 °C and 1650 °C are very porous and have relatively faceted fine grains, that the three ceramics RSPS-ed at 1700 °C, 1750 °C, and 1800 °C are still porous, but with rather isolated pores and already with fine–medium faceted grains, and that the two ceramics RSPS-ed at 1850 °C and 1900 °C are already essentially dense and with medium and coarse faceted grains, respectively. These SEM observations indicate that 1850 °C is the optimal RSPS temperature for the shaker-milled ZrH_2+2B powder mixture. Note that 1800 °C has been reported for the RSPS of a wet-milled ZrH_2+2B powder mixture [28], but measured with a radial pyrometer which underestimates the actual temperature of conductive samples relative to an axial pyrometer [41,42].

Fig. 7 shows the relative density (Fig. 7A), as measured by the Archimedes method, and the hardness (Fig. 7B), as measured by Vickers indentation, of all ZrB_2 ceramics quantitatively confirming the above conclusion that RSPS is optimal at 1850 °C. Certainly, it can be seen in Fig. 7 that both the degree of densification and the hardness increase with increasing RSPS temperature, and that the latter scales directly

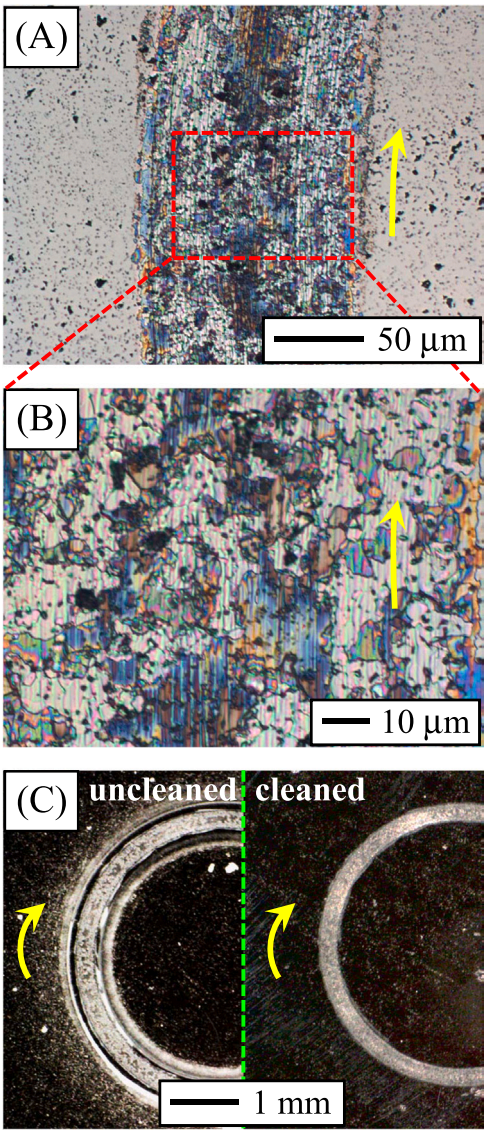

Fig. 14. (A-B) OM images of the residual wear tracks in the ZrB_2 ceramic fabricated by RSPS at 1850 °C (for 5 min under 75 MPa) from the shaker-milled ZrH_2+2B powder mixture. (C) DOM images of the uncleaned and cleaned wear tracks. The arrows denote the sliding direction.

with the former. Specifically, it can be seen that RSPS of the shaker-milled ZrH_2+2B powder mixture yields ZrB_2 ceramics having reached the boundary between the initial and intermediate sintering regimes at 1500 °C and 1550 °C (~70% dense with <6 GPa hardness), the middle stage of the intermediate sintering regime at 1600 °C (~82% dense with ~10 GPa hardness), the later stage of the intermediate sintering regime at 1650 °C (~88% dense with ~13 GPa hardness), the earlier stage of the final sintering regime at 1700 °C (~92% dense with ~17 GPa hardness), the middle stage of the final sintering regime at 1750 °C and 1800 °C (~95% dense with ~18–19 GPa hardness), and finally the later stage of the final sintering regime at and above 1850 °C (~98.5% dense with ~20 GPa hardness). Consequently, it is clear that RSPS at 1850 °C maximises hardness, and that RSPS temperatures above 1850 °C are no longer beneficial in terms of hardness and, however, are detrimental in terms of microstructural coarsening (which in turn is known to degrade the wear resistance of polycrystalline ceramics [10,43–49]).

3.3. Comparison with RSPS from ZrH_2+2B without pre-milling and with SPS from ZrB_2

To univocally compare the RSPS from the shaker-milled ZrH_2+2B powder mixture with other sintering approaches, three reference ceramics were also fabricated at 1850 °C for 5 min under 75 MPa pressure, one by RSPS from the simply-mixed ZrH_2+2B powder mixture and two by SPS of a typical commercial ZrB_2 powder both without and with the same shaker pre-milling as the ZrH_2+2B powder mixture. Figs. 8 and 9 show FE-SEM images and the XRD patterns of these three powders, respectively, showing that the first comprises a mixture of fine+coarse crystalline ZrH_2 particles (~1–15 μm) and submicrometric (<1 μm) amorphous B particles, that the second comprises micrometric ZrB_2 particles (~2–3 μm, as indicated by the manufacturer), and that the third comprises micrometric agglomerates of ultrafine ZrB_2 particles plus micrometric particles not refined during shaker milling. Therefore, despite the large ZrH_2 particle size, the ZrH_2+2B powder mixture milled better than the ZrB_2 powder, probably because ZrH_2 is more brittle than ZrB_2.

Figs. 10 and 11 show the XRD patterns and SEM images of the fracture surface of the three resulting ceramics, respectively. It can be seen in Fig. 10 that the ceramic RSPS-ed from the simply-mixed ZrH_2+2B powder mixture only contains ZrB_2, indicating that 1850 °C is a sufficiently high temperature to also complete the reaction of ZrB_2 formation from coarse particulate reactants. The ceramics SPS-ed from the commercial and shaker-milled ZrB_2 powders have the expected phase compositions, the former only with ZrB_2 and the latter with ZrB_2 plus traces of ZrO_2 impurities. The existence of ZrO_2 is again attributable to the slight spontaneous passivation of the ultrafine/fine ZrB_2 particles prior to SPS. Interestingly, the fact that the ZrH_2+2B powder mixture milled better than the ZrB_2 powder, and therefore that its greater specific surface area must have resulted in greater formation of passivating oxide, together with the existence of only tetragonal ZrO_2 impurities in the ceramic RSPS-ed at 1850 °C from the former but both monoclinic and tetragonal ZrO_2 impurities in the ceramic SPS-ed at 1850 °C from the latter, suggest that the H_2 released during the ZrH_2 decomposition could have partially reduced the passivating oxide layers. More importantly, it can be seen in Fig. 11 that the three are, to a greater or lesser extent, very porous and with coarse-grained microstructures. Of the three, the one SPS-ed from the commercial ZrB_2 powder is the least dense and coarse-grained, attributable to the very poor densifiability of micrometric ZrB_2 [6,7]. The one SPS-ed from the shaker-milled ZrB_2 powder is the densest, but not the coarsest grained, attributable to the enhanced sinterability of refined ZrB_2 [50,51]. Lastly, the one RSPS-ed from the simply-mixed ZrH_2+2B powder mixture is the coarsest grained, but not the densest, attributable to the very large ZrH_2 particle size. Their relative densities measured by the Archimedes method, which have also been included in Fig. 7A for the sake of comparison, are as low as ~83.3% for the one RSPS-ed from the simply-mixed ZrH_2+2B powder mixture, ~76.7% for the one SPS-ed from the commercial ZrB_2 powder, and ~86.7% for the one SPS-ed from shaker-milled ZrB_2 powder. Therefore, the three have reached only the intermediate sintering regime, but the first its middle stage, the second its early stage, and the third its later stage according to the classification used above. Also, it can be seen in Fig. 7B that, owing to their low degrees of densification, these three ZrB_2 ceramics are comparatively much softer than the counterpart RSPS-ed at 1850 °C from the shaker-milled ZrH_2+2B powder mixture (~11.1, 6.0, and 11.8 GPa, respectively, *vs* 20 GPa).

Therefore, it is evident that RSPS from the shaker-milled ZrH_2+2B powder mixture is the best choice of the four processing approaches. Indeed, comparatively it achieved at 1600 °C, ~1575 °C, and 1650 °C the same degrees of densification as RSPS at 1850 °C from the simply-mixed ZrH_2+2B powder mixture and SPS at 1850 °C from both the commercial and shaker-milled ZrB_2 powders, respectively. Importantly, neither RSPS nor high-energy ball-milling alone is sufficient to achieve

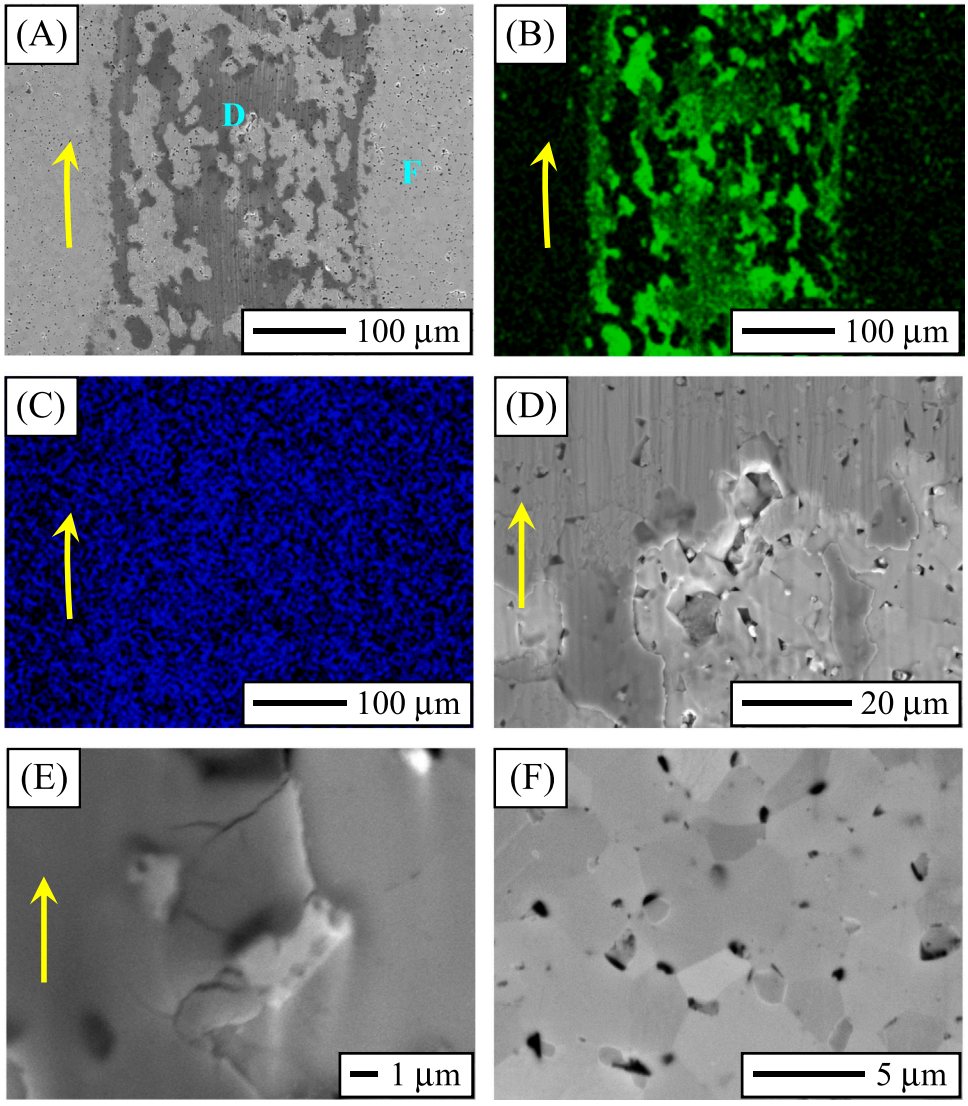

Fig. 15. (A) Low-magnification SEM image and the corresponding elemental composition maps of (B) O and (C) C acquired by EDS of the residual wear tracks in the ZrB_2 ceramic fabricated by RSPS at 1850 °C (for 5 min under 75 MPa) from the shaker-milled ZrH_2+2B powder mixture. SEM images (D) of the damage inside the wear tracks (taken in the zone denoted as D in (A)), (E) of a zone of the tribolayer at higher magnification, and (F) of the polished surface outside the wear tracks (taken in the zone denoted as F in (A)). The arrows denote the sliding direction.

fully-dense ZrB_2 ceramics at 1850 °C. The synergistic combination of the two is necessary to achieve complete densification at that temperature, the former because it generates exothermic reaction heat useful for sintering (Fig. 4), and the latter because it refines, mechanically activates, and uniformly mixes the particles of the reactants (Figs. 1 and 3) making them more sinterable. Lastly, using ZrH_2 as reactant would also have helped because it is easy to mill and because the H_2(g) resulting from its decomposition during the sintering cycle could have partially reduced the oxide passivating layers.

3.4. Unlubricated sliding-wear behaviour

Fig. 12 shows FE-SEM images of the polished surface of the ZrB_2 ceramic RSPS-ed at 1850 °C (for 5 min under 75 MPa), which was chosen for the tribological study as it is the optimal of all the materials fabricated. It can be seen that, in perfect agreement with its XRD pattern (Fig. 5) and the SEM image of its fracture surface (Fig. 6H) presented above, it is essentially dense, and that it has a microstructure constituted by micrometric ZrB_2 grains plus finer ZrO_2 grains (lighter grains). Fig. 13 shows some relevant wear results for this ZrB_2 ceramic, tested against diamond under 40 N load for 1000 m of sliding. It can be seen in Fig. 13 A that there was ease of sliding, with a very low, flat, and smooth CoF even in the absence of external lubrication, suggesting the occurrence of little wear. The 3-D image of the worn surface of the ZrB_2 ceramic in Fig. 13B and the 2-D cross-sectional profiles in Fig. 13C confirm this expectation. Thus, it can be seen that the worn surface remained, even in the most damaged zones, relatively intact after 1000 m of sliding, and that the wear track is fairly narrow (~240–280 µm width) and shallow (~1–1.7 µm depth). The worn volume calculated from these wear track dimensions is only ~0.0017–0.0034 mm^3, which gives an SWR as low as ~$4.25–8.50 \cdot 10^{-8}$ $mm^3/(N \cdot m)$ and a wear resistance as high as ~$1.18–2.36 \cdot 10^7$ $(N \cdot m)/mm^3$. Therefore, according to these numbers and the standard graduation of engineering tribology [52–54], this ZrB_2 ceramic only underwent mild wear. In fact, under the particular wear conditions used here this monolithic ZrB_2 ceramic exhibited an SWR of the same order of magnitude (10^{-8} $mm^3/(N \cdot m)$) as some B_4C–based composites [49, 55–58].

Figs. 14 and 15 show OM/DOM and SEM/EDS images, respectively, of the wear tracks after 1000 m of sliding. As can be seen in Fig. 14A-B, the OM observations show that a discontinuous tribolayer was formed and that there was little damage, which is essentially in the form of superficial scratches parallel to the sliding direction with hardly any grain pull-out. It is likely that the tribolayer formed was continuous, and over time underwent cracking, delamination, and spalling. The DOM images in Fig. 14C support this hypothesis by showing that there is, despite the little damage in the ZrB_2 ceramic, loose wear debris, presumably chipped-off tribolayer areas, inside and outside the uncleaned

wear track but not in the cleaned wear track. Additionally, as can be seen in Fig. 15A-C, the elemental composition maps of O and C acquired by EDS demonstrate that the tribolayer is oxide, not material transferred from the diamond counter-ball, whose formation is then attributable to the surface oxidation of the contact zone as a consequence of the frictional heating generated during the sliding tests in air atmosphere. Also, Fig. 15D-E show that the oxide tribolayer is thin (because it is relatively "transparent" to the electron beam) and still with some cracks, further supporting that at some given time it must have covered the entire wear track. Nonetheless, the important point is that the oxide tribolayer contributed to minimising wear by preventing the long-lasting asperity contacts between the ZrB_2 ceramic and the diamond counter-ball, and by self-lubricating, thanks to its lower shear strength [53], the contact thus reducing the friction. The latter explains why the CoF is so low (*i.e.*, <0.1), and more typical of lubricated contacts than non-lubricated ones [53]. Finally, Fig. 15D and E confirm that there is only very minor ZrB_2 grain pull-out, that wear damage is essentially in the form of plastic grooves, and that the small pitted zones within the wear track are mostly from ZrO_2 pulled out due to its weaker cohesion with the ZrB_2 grains.

Therefore, the pattern of macro- and micro-damage indicates that this ZrB_2 ceramic underwent mild tribo-oxidative wear, first wearing mechanically by a slight plasticity-dominated two-body abrasion until an oxide tribolayer was formed, which dictated the onset of a slight oxidative wear. The tribolayer continued to wear first by plasticity-dominated two-body abrasion and then by microfracture-dominated two-body abrasion, which marked the onset of an additional slight three-body abrasion (likely dominated by microfracture for the still-remaining tribolayer and by plasticity for the bare worn surface). Notwithstanding the above, the remarkable result is that the monolithic ZrB_2 ceramic only underwent mild wear due to its high hardness and the protection and self-lubrication provided by the oxide tribolayer, and is thus a promising tribo-ceramic for engineering applications requiring wear resistance.

4. Conclusions

A study was conducted on the fabrication of monolithic ZrB_2 ceramics by RSPS from a ZrH_2+2B powder mixture subjected to shaker pre-milling, and then compared with other sintering approaches. Subsequently, the unlubricated sliding-wear behaviour against diamond of the optimally RSPS-ed ZrB_2 ceramic was also studied. Based on the experimental results and analyses, the following conclusions can be drawn:

1. Shaker milling, even for only 1 h, refines, mechanically activates, and uniformly mixes the ZrH_2 and B particles, thus resulting in a more sinterable ZrH_2+2B powder mixture.
2. The ZrH_2+2B powder mixture reactively densifies during the sintering cycle in the SPS furnace to yield a ZrB_2 ceramic, with the decomposition reaction of ZrH_2 occurring first, followed by the ZrB_2 formation reaction. The exothermic reaction heat generated is thus very useful for densification.
3. RSPS from the shaker-milled ZrH_2+2B powder mixture is optimal at 1850 °C (for 5 min under 75 MPa), already resulting in dense ZrB_2 ceramics with ~20 GPa hardness. RSPS at lower temperature results in non-dense (70–95%) and softer (<6.0–19 GPa) ZrB_2 ceramics, and RSPS at higher temperature causes undesirable microstructural coarsening without benefiting densification and hardness.
4. Fabrication of dense ZrB_2 ceramics benefits synergistically from the use of both RSPS and shaker pre-milling of the reactants. The combination of the two is more advantageous than separately, and also more than SPS both without and with shaker pre-milling of commercial ZrB_2 powders.
5. The optimally RSPS-ed ZrB_2 ceramic is resistant to the unlubricated sliding wear, exhibiting (*i*) a low SWR (~4.25–8.50·10^{-8} mm^3/(N·m)) when tested against diamond under 40 N load for 1000 m and (*ii*) little damage caused by mild tribo-oxidative wear in the form of a slight plasticity-dominated two-body abrasion with eventual formation and partial loss of a protective and self-lubricating oxide tribolayer. It is, therefore, a promising tribo-ceramic for engineering applications requiring wear resistance.

Declaration of Competing Interest

The authors declare that they have no known competing financial interests or personal relationships that could have appeared to influence the work reported in this paper.

Acknowledgements

The authors acknowledge the financial support provided by the Spanish Ministry of Science and Innovation under Grant no. PID2019-103847RJ-I00, Junta de Andalucía under Grant no. P18-RTJ-1972, and Junta de Extremadura under Grants nos. IB20017 and GR21170 (co-financed with FEDER funds).

References

[1] M.M. Opeka, I.G. Talmy, J.A. Zaykoski, Oxidation-based materials selection for 2000°C + hypersonic aerosurfaces: theoretical considerations and historical experience, J. Mater. Sci. 39 (19) (2004) 5887–5904.
[2] E. Wuchina, E. Opila, M. Opeka, W.G. Fahrenholtz, I. Talmy, UHTCs: ultra-high temperature ceramic materials for extreme environment applications, Interface 16 (4) (2007) 30–36.
[3] K. Upadhya, J.-M. Yang, W.P. Hoffmann, Materials for ultrahigh temperature structural applications, Am. Ceram. Soc. Bull. 76 (12) (1997) 51–56.
[4] W.G. Fahrenholtz, G.E. Hilmas, Ultra-high temperature ceramics: Materials for extreme environments, Scr. Mater. 129 (2017) 94–99.
[5] D. Ni, Y. Cheng, J. Zhang, J.-X. Liu, J. Zou, B. Chen, H. Wu, H. Li, S. Dong, J. Han, X. Zhang, Q. Fu, G.-J. Zhang, Advances in ultra-high temperature ceramics, composites, and coatings, J. Adv. Ceram. 11 (1) (2022) 1–56.
[6] W.G. Fahrenholtz, G.E. Hilmas, I.G. Talmy, J.A. Zaykoski, Refractory diborides of zirconium and hafnium, J. Am. Ceram. Soc. 90 (5) (2007) 1347–1364.
[7] S.Q. Guo, Densification of ZrB_2-based composites and their mechanical and physical properties: a review, J. Eur. Ceram. Soc. 29 (6) (2009) 995–1011.
[8] N.P. Padture, Advanced structural ceramics in aerospace propulsion, Nat. Mater. 15 (2016) 804–809.
[9] R. Telle, L.S. Sigl, K. Takagi, Boride-Based hard materials. Handbook of Ceramic Hard Materials, Wiley-VCH Verlag GmbH,, Weinheim, Germany, 2000, pp. 802–945.
[10] X. Wang, N.P. Padture, H. Tanaka, A.L. Ortiz, Wear-resistant ultra-fine-grained ceramics, Acta Mater. 53 (2) (2005) 271–277.
[11] K. Umeda, Y. Enomoto, A. Mitsui, K. Mannami, Friction and wear of boride ceramics in air and water, Wear 169 (1) (1993) 63–68.
[12] S. Chakraborty, A.R. Mallick, D. Debnath, P.K. Das, Densification, mechanical and tribological properties of ZrB_2 by SPS: effect of pulsed current, Int. J. Refract. Met. Hard Mater. 48 (2015) 150–156.
[13] J. He, Y. Cao, Z. Li, Y. Wang, Study of tribological properties of polymer derived ZrB_2-SiC ceramics, Ceram. Int. 44 (13) (2018) 15627–15630.
[14] K. Sonber, K. Raju, T.S.R.C. Murthy, K. Sairam, A. Nagaraj, S. Majumdar, V. Kain, Friction and wear properties of zirconium diboride in sliding against WC ball, Int. J. Refract. Met. Hard Mater. 76 (2018) 41–48.
[15] J. He, Y. Cao, Y. Zhang, Y. Wang, Mechanical properties of ZrB_2–SiC ceramics prepared by polymeric precursor route, Ceram. Int. 44 (6) (2018) 6520–6526.
[16] S. Mondal, S. Chakraborty, S. Das, Mechanical and tribological behavior of ZrB_2-TiB_2 system prepared by mechanical activation spark plasma sintering technique, J. Mater. Eng. Perform. 27 (11) (2018) 6040–6048.
[17] T.R. Paul, M.K. Mondal, M. Mallik, Dry sliding wear response of ZrB_2-20vol% $MoSi_2$ composite, Mater. Today Proc. 5 (2 Part 2) (2018) 7174–7183.
[18] M. Mallik, P. Mitra, N. Srivastava, A. Narain, S.G. Dastidar, A. Singh, T.R. Paul, Abrasive wear performance of zirconium diboride based ceramic composite, Int. J. Refract. Met. Hard Mater. 79 (2019) 224–232.
[19] D. Medveď, J. Balko, R. Sedlák, A. Kovalčíková, I. Shepa, A. Naughton-Duszová, E. Bączek, M. Podsiadło, J. Dusza, Wear resistance of ZrB_2 based ceramic composites, Int. J. Refract. Met. Hard Mater. 81 (2019) 214–224.
[20] M. Ivor, D. Medved, M. Vojtko, A. Naughton-Duszova, L. Marciniak, J. Dusza, Nanoindentation and tribology of ZrB_2 based luminescent ceramics, J. Eur. Ceram. Soc. 40 (14) (2020) 4901–4908.
[21] N.L. Savchenko, Y.A. Mirovoy, A.S. Buyakov, A.G. Burlachenko, M.A. Rudmin, I. N. Sevostyanova, S.P. Buyakova, S.Y. Tarasov, Adaptation and self-healing effect of tribo-oxidizing in high-speed sliding friction on ZrB_2-SiC ceramic composite, Wear 446–447 (2020), 203204.
[22] H. Chen, Z. Wu, W. Hai, L. Liu, W. Sun, Tribo-oxidation and tribological behaviour of ZrB_2-20%vol SiC composites coupled with WC and Al_2O_3 at high temperatures, Wear 464–465 (2021), 203534.

[23] T.R. Paul, M.K. Mondal, M. Mallik, Abrasive wear performance and wear map of ZrB_2-$MoSi_2$-SiC_w composites, J. Eur. Ceram. Soc. 41 (6) (2021) 3227–3251.
[24] D. Sciti, S. Guicciardi, L. Zoli, S. Failla, C. Melandri, Dry sliding wear behaviour of ZrB_2-based ceramics: self-mated and cross coupling with alumina, J. Eur. Ceram. Soc. 42 (14) (2022) 6335–6346.
[25] M. Brochu, B.D. gaunt, L. Boyer, R.E. Loehman, Pressureless reactive sintering of ZrB_2 ceramic, J. Eur. Ceram. Soc. 29 (8) (2009) 1493–1499.
[26] J.M. Lonergan, W.G. Fahrenholtz, G.E. Hilmas, Sintering mechanisms and kinetics for reaction hot-pressed ZrB_2, J. Am. Ceram. Soc. 98 (8) (2015) 2344–2351.
[27] R. Licheri, C. Musa, R. Orrù, G. Cao, Influence of the heating rate on the in situ synthesis and consolidation of ZrB_2 by reactive spark plasma sintering, J. Eur. Ceram. Soc. 35 (4) (2015) 1129–1137.
[28] S. Guo, T. Nishimura, Y. Kagawa, Preparation of zirconium diboride ceramics by reactive spark plasma sintering of zirconium hydride–boron powders, Scr. Mater. 65 (11) (2011) 1018–1021.
[29] R. Orrù, G. Cao, Comparison of reactive and non-reactive spark plasma sintering routes for the fabrication of monolithic and composite ultra high temperature ceramics (UHTC) materials, Materials 6 (5) (2013) 1566–1583.
[30] V. Zamora, A.L. Ortiz, F. Guiberteau, M. Nygren, L.L. Shaw, On the crystallite size refinement of ZrB_2 by high-energy ball-milling in the presence of SiC, J. Eur. Ceram. Soc. 31 (13) (2011) 2407–2414.
[31] V. Zamora, A.L. Ortiz, F. Guiberteau, M. Nygren, On the enhancement of the spark-plasma sintering kinetics of ZrB_2–SiC powder mixtures subjected to high-energy co-ball-milling, Ceram. Int. 39 (4) (2013) 4191–4204.
[32] B. Núñez-González, A.L. Ortiz, F. Guiberteau, M. Nygren, Spark-plasma-sintering kinetics of ZrC–SiC powder mixtures subjected to high-energy co-ball-milling, Ceram. Int. 39 (8) (2013) 9691–9697.
[33] V. Zamora, F. Guiberteau, A.L. Ortiz, Effect of high-energy ball-milling on the spark plasma sinterability of ZrB_2 with transition metal disilicides, J. Eur. Ceram. Soc. 40 (15) (2020) 5020–5028.
[34] V. Zamora, F. Guiberteau, A.L. Ortiz, Fabrication of ultrafine-grained ZrC–Co cemented carbides with superior sliding-wear resistance from micrometre starting powders, Ceram. Int. 47 (17) (2021) 24831–24840.
[35] J. López-Arenal, B.M. Moshtaghioun, F.L. Cumbrera, D. Gómez-García, A.L. Ortiz, Powder-metallurgy fabrication of ZrB_2–hardened Zr_3Al_2 intermetallic composites by high-energy ball-milling and reactive spark-plasma sintering, J. Mater. Res. Technol. 21 (2022) 617–626.
[36] C. Suryanarayana, Mechanical alloying and milling, Prog. Mat. Sci. 46 (1–2) (2001) 1–184.
[37] P.R. Soni, Mechanical Alloying, Fundamental and Applications, Cambridge International Science Publishing,, Cambridge, UK, 2001.
[38] A.L. Ortiz, F. Sánchez-Bajo, V.M. Candelario, F. Guiberteau, Comminution of B_4C powders with a high-energy mill operated in air in dry or wet conditions and its effect on their spark-plasma sinterability, J. Eur. Ceram. Soc. 37 (13) (2017) 3873–3884.
[39] S. Ran, S.G. Huang, O. Van der Biest, J. Vleugels, High-strength ZrB_2–based ceramics prepared by reactive pulsed electric current sintering of ZrB_2–ZrH_2 powders, J. Eur. Ceram. Soc. 32 (10) (2012) 2537–2543.
[40] W.G. Fahrenholtz, Reactive processing in ceramic-based systems, Int. J. Appl. Ceram. Technol. 3 (1) (2006) 1–12.
[41] O. Guillon, J. Gonzalez-Julian, B. Dargatz, T. Kessel, G. Schierning, J. Räthel, M. Herrmann, Field-assisted sintering technology/spark plasma sintering: mechanisms, materials, and technology developments, Adv. Eng. Mater. 16 (7) (2014) 830–849.
[42] C. Manière, A. Pavia, L. Durand, G. Chevallier, K. Afanga, C. Estournès, Finite-element modeling of the electro-thermal contacts in the spark plasma sintering process, J. Eur. Ceram. Soc. 36 (3) (2016) 741–748.
[43] S.-J. Cho, B.J. Hockey, B.R. Lawn, S.J. Bennison, Grain-size and *R*-curve effects in the abrasive wear of alumina, J. Am. Ceram. Soc. 72 (7) (1989) 1249–1252.
[44] O. Borrero-Lopez, A.L. Ortiz, F. Guiberteau, N.P. Padture, Microstructural design of sliding-wear-resistant liquid-phase-sintered SiC: an overview, J. Eur. Ceram. Soc. 27 (11) (2007) 3351–3357.
[45] O. Borrero-Lopez, A.L. Ortiz, A.D. Gledhill, F. Guiberteau, T. Mroz, L.M. Goldman, N.P. Padture, Microstructural effects on the sliding wear of transparent magnesium-aluminate spinel, J. Eur. Ceram. Soc. 32 (12) (2012) 3143–3149.
[46] E. Ciudad, O. Borrero-López, A.L. Ortiz, F. Guiberteau, Microstructural effects on the sliding wear resistance of pressureless liquid-phase-sintered SiC under diesel fuel, J. Eur. Ceram. Soc. 33 (4) (2013) 879–885.
[47] D. Bertagnoli, O. Borrero-López, F. Rodríguez-Rojas, F. Guiberteau, A.L. Ortiz, Effect of processing conditions on the sliding-wear resistance of ZrC triboceramics fabricated by spark-plasma sintering, Ceram. Int 41 (10 Part B) (2015) 15278–15282.
[48] E. Sánchez-González, O. Borrero-López, F. Guiberteau, A.L. Ortiz, Microstructural effects on the sliding-wear resistance of ZrC-$MoSi_2$ triboceramics fabricated by spark-plasma sintering, J. Eur. Ceram. Soc. 36 (13) (2016) 3091–3097.
[49] C. Ojalvo, V. Zamora, R. Moreno, F. Guiberteau, A.L. Ortiz, Transient liquid-phase assisted spark-plasma sintering and dry sliding wear of B_4C ceramics fabricated from B_4C nanopowders, J. Eur. Ceram. Soc. 41 (3) (2021) 1869–1877.
[50] V. Zamora, A.L. Ortiz, F. Guiberteau, M. Nygren, Crystal-size dependence of the spark-plasma-sintering kinetics of ZrB_2 ultra-high-temperature ceramics, J. Eur. Ceram. Soc. 32 (2) (2012) 271–276.
[51] V. Zamora, A.L. Ortiz, F. Guiberteau, M. Nygren, Spark-plasma sintering of ZrB_2 ultra-high-temperature ceramics at lower temperature via nanoscale crystal refinement, J. Eur. Ceram. Soc. 32 (10) (2012) 2529–2536.
[52] K. Adachi, K. Kato, N. Chen, Wear map of ceramics, Wear 203–204 (1997) 291–301.
[53] B. Bhushan, Modern Tribology Handbook, CRC Press, Boca Raton, USA, 2001.
[54] G.W. Stachowiak, A.W. Batchelor. Engineering Tribology, 3rd ed., Elsevier Butterworth-Heinemann,, Oxford, UK, 2005.
[55] C. Ojalvo, E. Sánchez-González, F. Guiberteau, O. Borrero-López, A.L. Ortiz, Improving the dry sliding-wear resistance of B_4C ceramics by transient liquid-phase sintering, J. Eur. Ceram. Soc. 40 (15) (2020) 15286–15292.
[56] V. Zamora, C. Ojalvo, F. Guiberteau, O. Borrero-López, A.L. Ortiz, Ultra-low wear B_4C-SiC-MoB_2 composites fabricated at lower temperature from B_4C with $MoSi_2$ additives, J. Eur. Ceram. Soc. 41 (16) (2021) 68–75.
[57] V. Zamora, F. Guiberteau, O. Borrero-López, A.L. Ortiz, Ultra-low temperature spark plasma sintering of super wear-resistant hard B_4C composites, Scr. Mater. 211 (2022), 114516.
[58] V. Zamora, F.J. Martínez-Vázquez, F. Guiberteau, A.L. Ortiz, Unlubricated sliding wear of B_4C composites spark-plasma sintered with Si aids and of their reference B_4C monoliths, J. Eur. Ceram. Soc. 43 (3) (2023) 814–823.